VISUALIZING LONG-RANGE SEVERE THUNDERSTORM ENVIRONMENT GUIDANCE FROM CFSv2

BY GREGORY W. CARBIN, MICHAEL K. TIPPETT, SAMUEL P. LILLO, AND HAROLD E. BROOKS

The CFSv2 Climate Forecast System is used to demonstrate new methods of visualizing large sets of model forecasts, with the application of extended-range forecasts for environments conducive to severe thunderstorms.

After violent tornadoes across the South and Midwest of the United States in 2011 and 2012, questions arose as to whether the National Oceanic and Atmospheric Administration's (NOAA) National Weather Service (NWS) could provide seasonal severe thunderstorm outlooks analogous to seasonal hurricane outlooks (Camargo et al. 2007). While NOAA provides climatological information of severe weather through its national Storm Prediction Center (SPC) and National Centers for Environmental Information (NCEI), as well as monthly and seasonal temperature and precipitation outlooks from the Climate Prediction Center (CPC), severe thunderstorm forecasts beyond 8 days are not part of any operational product suite. However, emerging science suggests that low-frequency (time scales from a week to months) modes of climate variability (e.g., the Pacific–North America pattern) may modulate severe weather activity and severe weather environments (Allen et al. 2015; Tippett et al. 2015a). Given these relationships, if forecast models are able to simulate such low-frequency modes of variability, they may also be able to capture the modulation of severe weather environments and thereby provide extended-range guidance for severe weather activity. A particular challenge of severe weather is that it occurs on short time scales, unlike persistent climate phenomena, such as drought. Consequently, model guidance for severe weather needs to contain information about severe weather

AFFILIATIONS: CARBIN—NOAA/National Weather Service/Storm Prediction Center, Norman, Oklahoma; TIPPETT—Department of Applied Physics and Applied Mathematics, Columbia University, New York, New York, and Center of Excellence for Climate Change Research, Department of Meteorology, King Abdulaziz University, Jeddah, Saudi Arabia; LILLO—Cooperative Institute for Mesoscale Meteorological Studies, University of Oklahoma, Norman, Oklahoma; BROOKS—NOAA/OAR/National Severe Storms Laboratory, Norman, Oklahoma
CORRESPONDING AUTHOR: Gregory Carbin, NOAA/NWS/Weather Prediction Center, 5830 University Research Court, College Park, MD 20740
E-mail: gregory.carbin@noaa.gov

The abstract for this article can be found in this issue, following the table of contents.
DOI:10.1175/BAMS-D-14-00136.1

In final form 7 August 2015

environments on daily or shorter time scales. The challenge for forecasters is how to effectively use large numbers of model forecasts to reliably predict inherently rare, high-impact events days in advance.

Given the significant societal impacts severe thunderstorms and tornadoes pose, the authors are collaborating on methods to extend the range of forecasts for these events. Here we begin to apply the longer-range (up to 45 days) forecasts available from the Climate Forecast System, version 2 (CFSv2), to the daily severe weather prediction challenge. Our strategy for identifying model output of interest to forecasters is as follows. An indication of potential predictability is when multiple consecutive forecasts exhibit similar outcomes, indicating that forecast outcomes are systematic responses to the evolving initial conditions. We would argue that it is reasonable to expect potential predictability to be a necessary, though not sufficient, requirement for achievable predictability and forecast skill. One approach we describe here reveals a relatively consistent potential predictability limit of around 7 days for daily-scale significant severe weather events occurring from late March to April 2014, when CFSv2 output is consolidated into single-day severe weather forecasts. Another approach, using run-cumulative information from CFSv2 long-lead forecasts to detect consistent anomalies in the forecasts, shows greater potential for skillful longer-lead forecasts of severe weather activity. Robust verification of these approaches is beyond the scope of this paper. The concepts described, however, naturally lead to establishing a baseline climatology through application of reanalysis and reforecasts to further assess the predictability of regimes supportive of severe thunderstorms on longer time scales (beyond the current 1-week limit), including events occurring over multiple days.

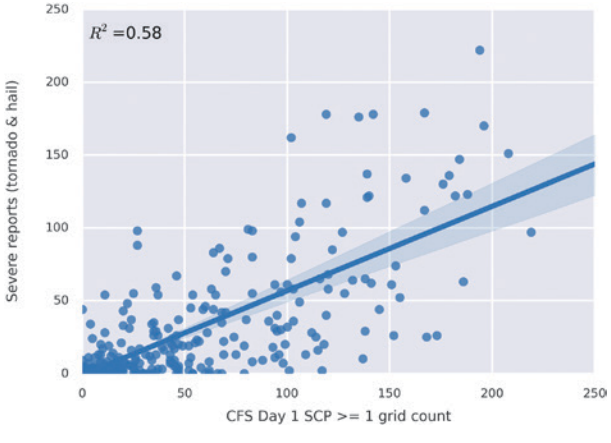

Fig. 1. The relationship of all 2014 day 1 CFS forecasts of convective day grid counts of average SCP ≥ 1 (*x* axis) to convective day tornado and hail reports (*y* axis). Day 1 CFSv2 forecasts of 24-h average SCP are composed of 6-h grids from 12- to 36-h forecasts and are used for verification. The coefficient of determination of 0.58 (upper left) and 95% confidence interval (shaded) are shown.

OVERVIEW OF CFS. The National Centers for Environmental Prediction's CFSv2 became operational in March 2011 (Saha et al. 2014). The CFSv2 is a global spectral model with coupled ocean–sea ice–land and atmosphere processes. The Climate Data Assimilation System, version 2 (CDASv2; a real-time continuation of the Climate Forecast System Reanalysis), is used to initialize operational CFSv2 runs (Saha et al. 2014). The CFSv2 has 64 vertical sigma-pressure hybrid layers and an equivalent horizontal grid spacing of approximately 100 km (T126).

CFSv2 output is available from 16 model runs per day. Four of those runs are forecasts out to 9 months, three runs are forecasts for one season, and nine runs are 45-day forecasts. The CFSv2 parameters used in this study are taken from the ensemble mean of the four 0000 UTC model runs available in 6-h time steps out to 45 days. The four 0000 UTC model run ensemble membership consists of a control run and three perturbed members generated from differences between the current and previous initial model states and multiplied control factors (W. Wang, NOAA, 2015, personal communication).

While the range (resolution) of the CFSv2 may seem too long (coarse) for use in predicting the mesoscale aspects of severe thunderstorm events, the CFSv2 is capable of capturing climate signals (e.g., Kirtman et al. 2009). Using time-lagged ensemble forecasts from this modeling system may allow the generation of potentially useful longer-range predictions of environments conducive to severe thunderstorms and tornadoes. These environments are defined by high levels of convective available potential energy (CAPE), strong low-level storm-relative helicity (SRH), and strong deep-layer vertical wind shear, or bulk wind difference (BWD; Doswell 1980; Brooks et al. 2003; Thompson et al. 2003, 2007; Grams et al. 2012). To depict synoptic-scale regimes potentially supportive of severe thunderstorms, we analyze daily averages (from 1200 to 1200 UTC in 6-h intervals) of a derived parameter, the supercell composite parameter (SCP), that combines the fields of CAPE, SRH, and BWD from the CFSv2 over the contiguous United States (CONUS).

OVERVIEW OF CFSV2 SCP. The SCP [Eq. (1)] is a normalized index developed to define atmospheric

environments with adequate instability, 0–3-km SRH, and deep-layer vertical shear to support organized thunderstorms, usually in the form of supercells (Thompson et al. 2003, 2007). The formulation used here is slightly modified from the index defined by Thompson et al. (2003). Specifically, a 0–180-hPa-layer "most unstable" CAPE is taken directly from CFSv2 output and bulk shear (or BWD) is computed from the u and v winds between the model's 0–30-hPa-above-ground layer and 500 hPa. SCP values of 1 or higher are associated with environments conducive to thunderstorm updraft persistence and rotation. The value of SCP is that it can be easily derived from near-real-time high-resolution mesoanalysis data and from longer-range forecast grids, such as the CFSv2. Drawbacks include the SCP not being an explicit predictor of supercells and clearly not accounting for an array of other complex processes involved in the development of severe storms (Doswell and Schultz 2006). Nonetheless, the use of severe weather indices in defining severe thunderstorm climatologies, and in severe weather prediction, has been documented in a number of studies (Brooks et al. 2003; Tippett et al. 2012b). In particular, Tippett et al. (2012b) showed that monthly CFSv2 forecasts of a tornado environment index (derived from convective precipitation and SRH) showed significant correlations with the observed monthly number of tornadoes across the CONUS:

$$\mathrm{SCP} = (\mathrm{CAPE}/1000\ \mathrm{J\ kg^{-1}}) \times (\mathrm{SRH}/50\ \mathrm{m^{-2}\ s^{-2}}) \times (\mathrm{BWD}/20\ \mathrm{m\ s^{-1}}). \quad (1)$$

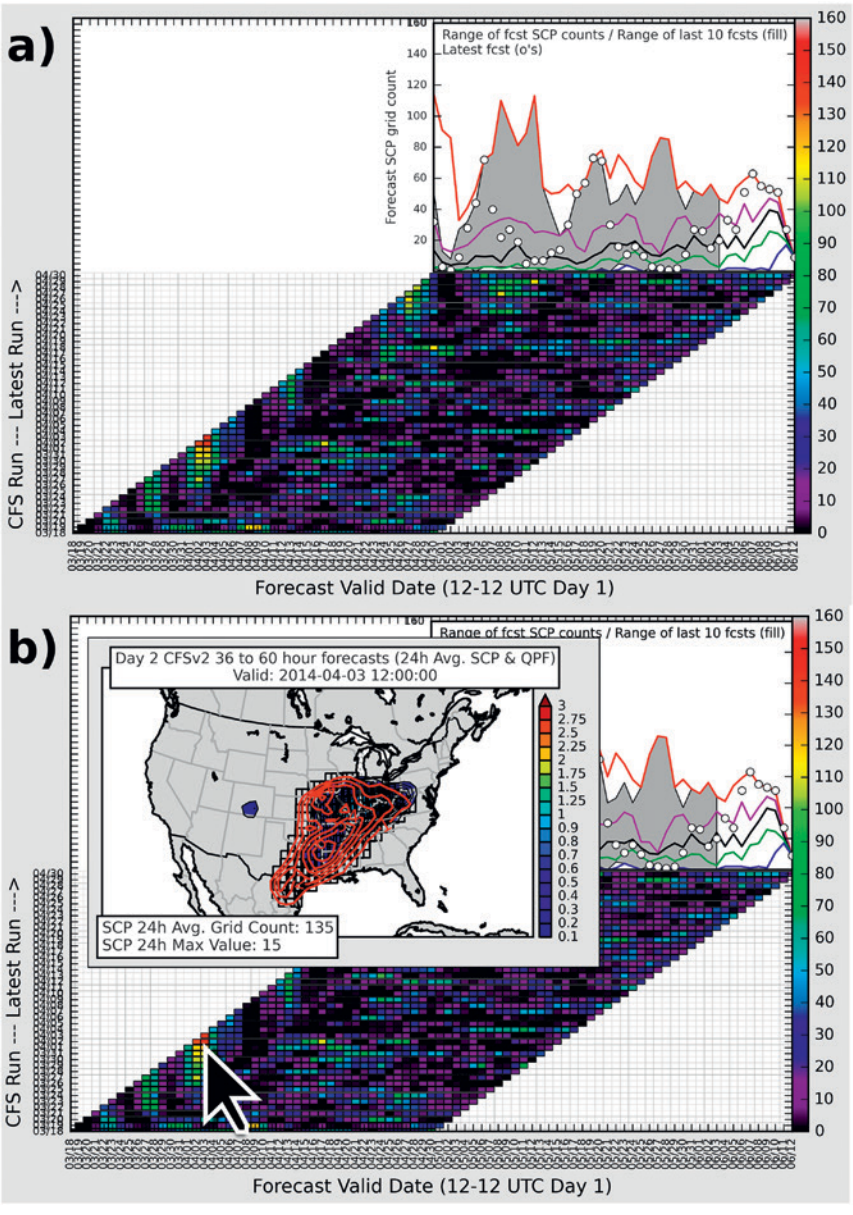

Fig. 2. (a) CFS SCP Chiclet Chart for the period from 18 Mar to 30 Apr 2014. (b) Example of mouseover on a day-2 chiclet with corresponding pop-up map valid on 3 Apr 2014.

VISUALIZATION OF CFSV2 SCP GRID COUNTS. A challenge in utilizing CFSv2 output for long-range forecasting is the ability to analyze, synthesize, and visualize the large amount of information available. The 45-day CFSv2 output is composed of a control run and three perturbed members with 6-h time steps. In all, over 4,000 individual forecasts per day are available from the system. One approach to managing this amount of forecast information has been to consolidate 6-h forecasts of SCP into daily-averaged SCP grid counts where the daily average is based on a "convective day" (as defined by SPC) from

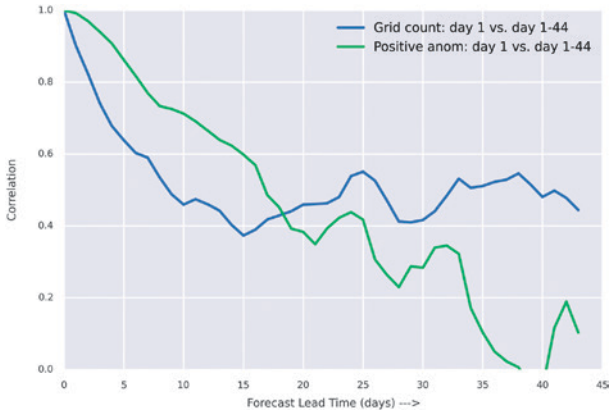

Fig. 3. Blue line depicts the correlation of 2014 CFSv2 SCP day-1 SCP grid counts with all other CFS grid-count forecasts from day 44 through day 1 (r = 1). Green line depicts a similar comparison but using time-lagged accumulation of SCP grid counts, and removing the 2-week running mean centered on each forecast day, to derive positive anomaly forecasts.

1200 to 1200 UTC the following calendar day. SCP forecasts can be further summarized by constructing the daily averages from the four-member CFSv2 ensemble mean, and further utilizing only those forecasts from the 0000 UTC model initialization. While this process does limit the amount of CFSv2 forecast information from other runs, it is deemed a reasonable approach for a proof-of-concept exercise. The relationship of 2014 CFSv2 forecasts of convective-day grid counts of average SCP ≥ 1 to convective day tornado and hail reports is shown in Fig. 1 for all verifying day-1 CFSv2 forecasts (day-1 CFSv2 forecasts of 24-h-average SCP are composed of 6-h grids from 12- to 36-h forecasts and are used for verification). There is a good association between forecast values of SCP and the number of tornado and hail reports.

Since December 2012, SPC forecasters have used an experimental web-based CFSv2 time-lagged ensemble chart, or "Chiclet Chart," to review 45-day forecasts of daily counts of the number of grid points with SCP ≥ 1 from the 0000 UTC CFSv2 ensemble mean over the CONUS. Using this approach, grid count forecasts from successive CFSv2 runs can be viewed where each pixel or "chiclet" on the chart corresponds to one convective day and the color of the chiclet represents the grid count of the daily average SCP ≥ 1 over a masked CONUS domain with 845 grid points. A similar display format, previously used in the context of El Niño–Southern Oscillation (ENSO) and rainfall forecasts (Barnston et al. 2012; Tippett et al. 2012a, 2015b), permits the visualization of multiple forecasts with the same valid time. The chart is constructed so that each successive CFSv2 run is stacked above prior runs, but staggered, so forecasts with identical valid times lie on the same x-axis coordinate (Fig. 2a). Vertical stripes of similar color indicate run-to-run consistency in SCP ≥ 1 grid counts (i.e., similar forecasts in terms of the areal extent of environments conducive to supercell thunderstorms across the CONUS). Forecasters can further interrogate the information presented in the web-based CFSv2 Chiclet Chart when they mouseover highlighted days to reveal CONUS maps of daily-averaged SCP grids (grid boxes and red contours), as well as the 24-h convective quantitative precipitation forecasts (QPF, color filled) to identify spatial patterns and locations where these fields overlap (Fig. 2b). By moving the mouse vertically along a column of highlighted days meeting SCP thresholds, the forecaster can visualize CFSv2 run-to-run consistency in the maps of severe storm environments, magnitude of daily average SCP, and convective QPF.

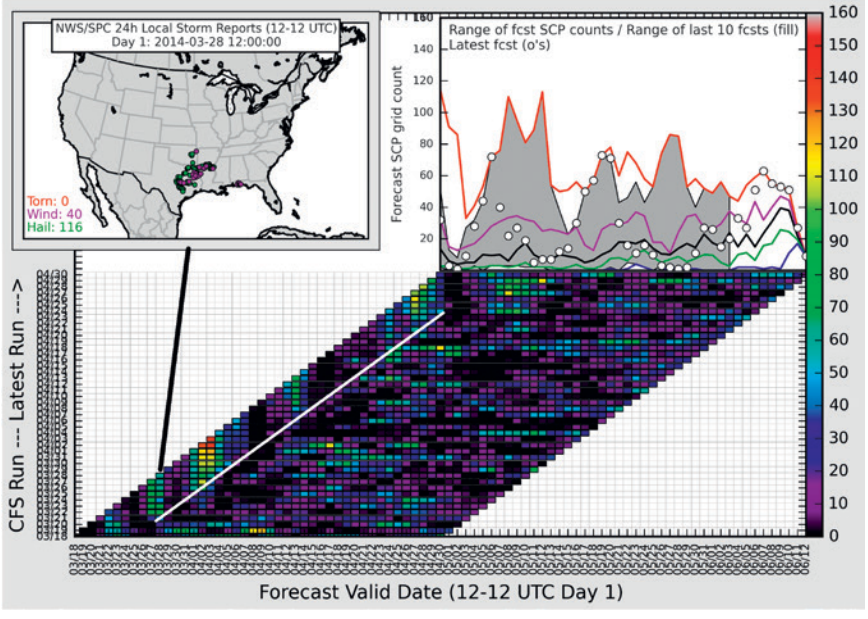

Fig. 4. Forecasts of SCP grid count (day 6–day 1) and resulting SPC storm reports (inset map in upper left) valid on 28 Mar 2014.

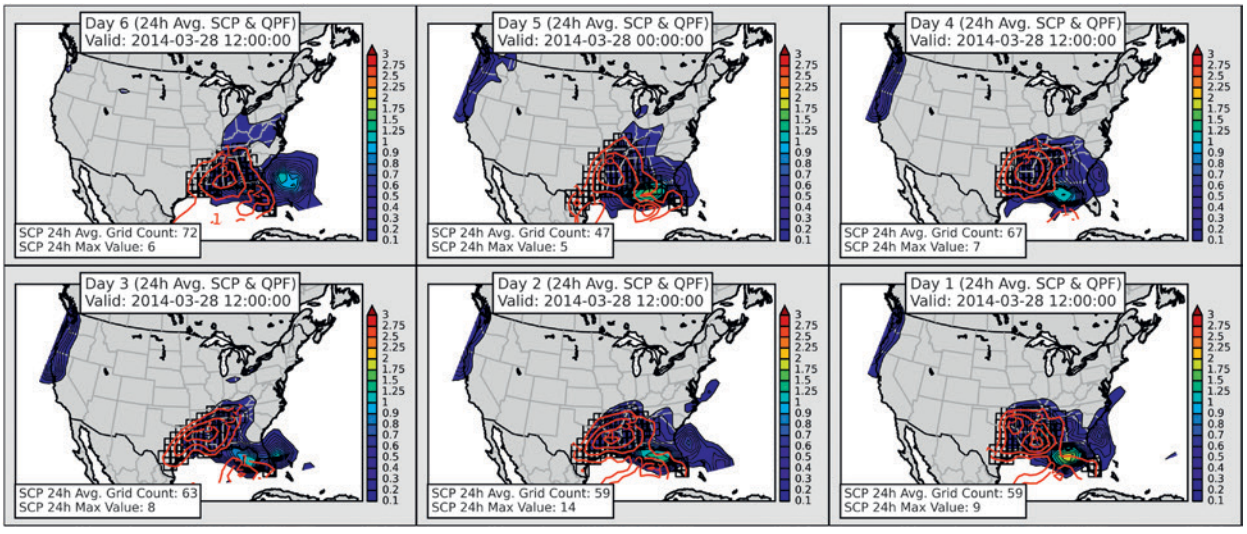

Fig. 5. Forecast maps of SCP grid count (contours) and convective QPF (colors) from day 6 to day 1 valid on 28 Mar 2014.

The Chiclet Chart depicts forecast consistency of SCP ≥ 1 grid counts when similarly colored chiclets appear in vertical sequences. Higher confidence can be given to severe weather potential when both the consistency and the areal coverage of daily-averaged SCP forecasts (from the CFSv2 ensemble mean) remain similar or increase as the valid date approaches. However, many multiday forecasts exist where a supportive regime is shown by successive highlighted chiclets, or a decay in an earlier high-end signal reappears at a later valid date, indicating uncertainty in the timing of events. Chiclet maxima sloping up and to the left indicate a trend toward a faster system (earlier event arrival), while maxima sloping up and to the right indicate a trend toward a slower system (later event arrival). For the multiday events indicated on the Chiclet Chart during this evaluation period, we will focus on the character of the forecasts from 6 days in advance to the day of the severe weather event (day 6–day 1 forecasts in SPC parlance).

Another graph contained within the Chiclet Chart (Fig. 2, top right) shows the forecast range of SCP ≥ 1 grid counts (*y* axis) from all available forecasts valid on the same day, from day 1 through day 44 (*x* axis). The quartile values of forecast grid counts are shown. The range between minimum and maximum counts for the 10 most recent forecasts is filled in gray, while the most recent forecast values are plotted as small white circles. This additional information can aid the forecaster in interpreting trends in CFSv2 output.

CFSV2 SCP EVALUATION FOR LATE MARCH AND APRIL 2014. Here we describe the character of CFSv2 daily CONUS forecasts for several severe weather events during the period from late March to April 2014. Of the 145 tornadoes reported

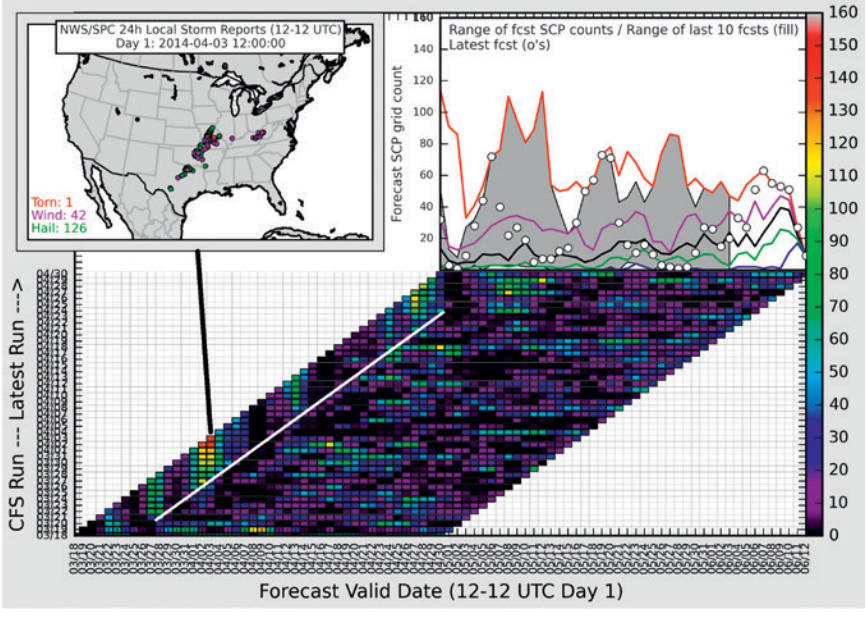

Fig. 6. As in Fig. 4, but for 3 Apr 2014.

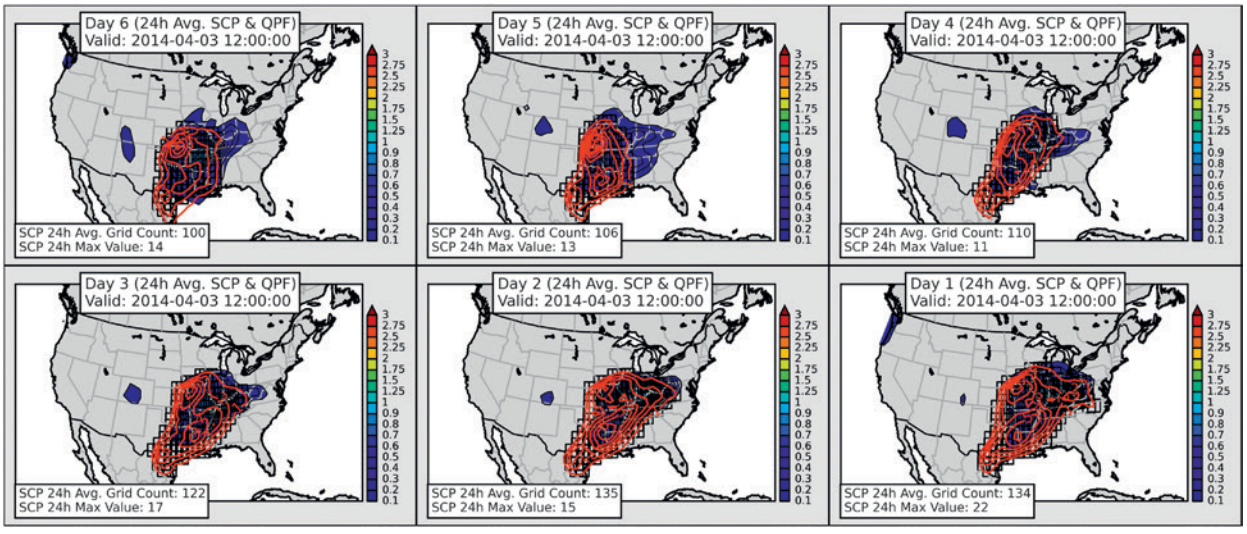

Fig. 7. As in Fig. 5, but for 3 Apr 2014.

in the CONUS during this period, 66 occurred on the 4 days reviewed here: 28 March, 3 April, 19 April, and 28 April. The most significant of these events occurred in late April, when a multiday tornado outbreak resulted in 84 tornadoes between 27 April and 30 April.

The correlation of CFSv2 SCP ≥ 1 day-1 grid-count forecasts with all other forecasts decreases as the forecast lead time increases (Fig. 3, blue line). Correlation values plateau around the 2-week mark and do not decrease further, likely a reflection of seasonality. The seasonal cycle is not removed in the correlation calculation. The decrease in forecast consistency is shown around the 1-week mark (a drop below a 0.5 correlation value) in Fig. 3, and also by the lack of similarly colored vertical lines beyond days 5–7 on the Chiclet Chart for late March–30 April 2014 (Fig. 2). To aid in delineating this transition from less consistent to more consistent forecasts, a sloped white line is drawn on subsequent Chiclet Charts evaluated below (Figs. 4, 6, 8, and 10).

Over 200 severe weather reports were plotted on the SPC report map valid for 28 March 2014 (Fig. 4, inset map). The potential for this particular event began to appear in CFSv2 forecasts around 21–22 March 2014. When viewing the evolution of the six forecasts leading up to 28 March, a consistent signal exists in both the areal coverage and the magnitude of SCP ≥ 1 grid counts (Fig. 5). A slight westward shift in convective QPF is evident as the forecast lead time decreases, indicating a trend toward slower eastward system evolution over time. The overall slower advance of this system is also supported by the multiday forecast (paired similarly colored chiclets) with 75 severe weather reports occurring primarily across the state of Missouri on 27 March 2014 (not shown).

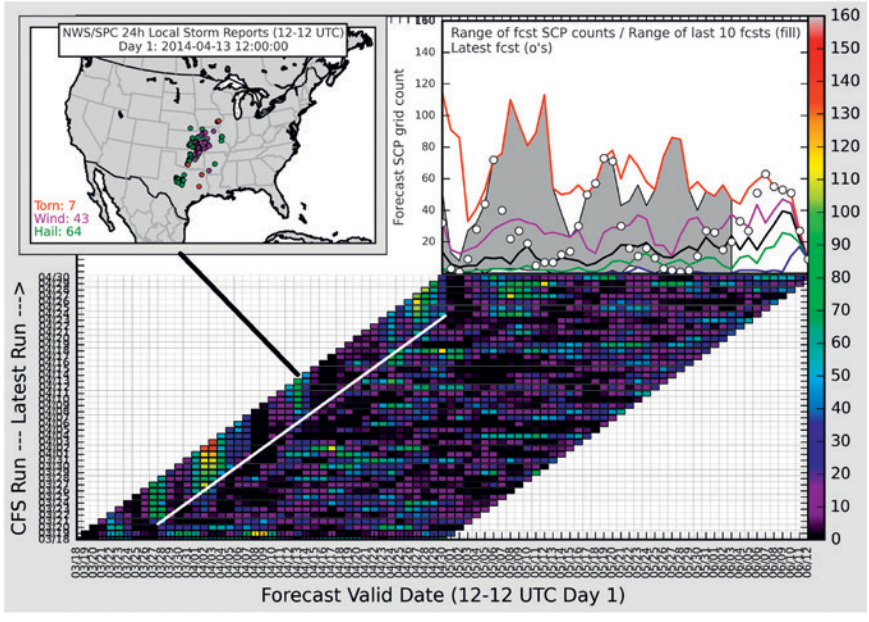

Fig. 8. As in Fig. 4, but for 13 Apr 2014.

The most active severe weather day of the first half

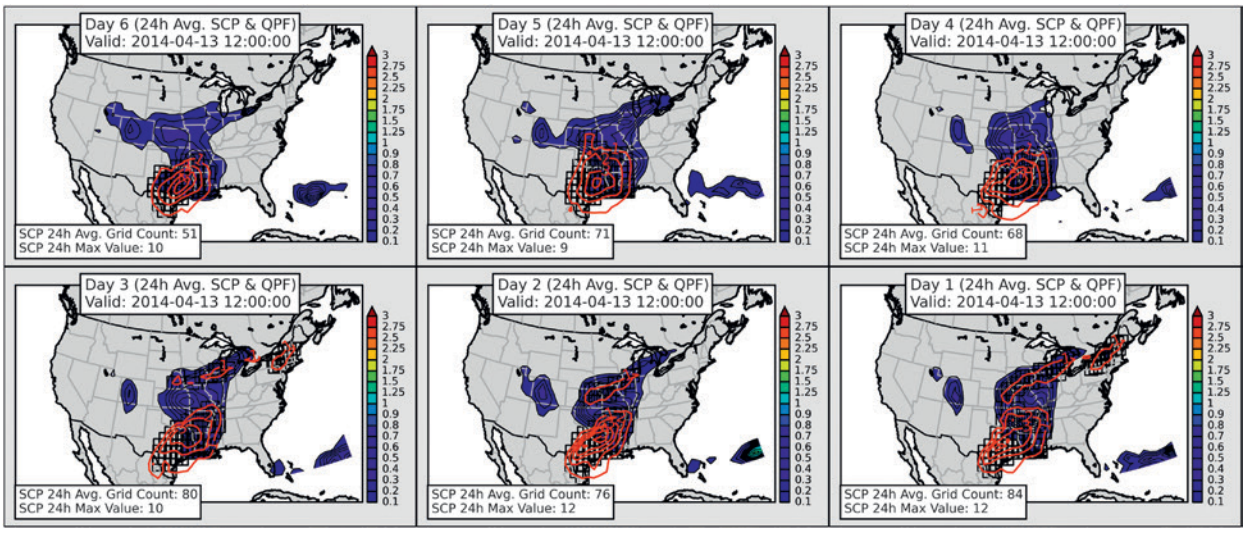

Fig. 9. As in Fig. 5, but for 13 Apr 2014.

of April 2014 occurred on the third day of the month with nearly 400 wind, hail, and tornado reports. There were 13 tornadoes reported on this day, including one rated EF2. The CFSv2 forecasts again provided an indication of severe weather potential across a multiday period beginning with forecasts initialized 6–7 days in advance (Fig. 6). Strong consistency exists in the day 6–day 1 forecast maps valid for 3 April 2014 (Fig. 7). An additional trend supporting greater confidence in a significant severe weather episode is the steady increase in SCP ≥ 1 grid counts, from 100 in the day-6 forecast to 135 in the day-2 forecast (Figs. 6 and 7). Only subtle changes are evident in the centroid of the 24-h convective QPF signal from one run to the next with this centroid also corresponding closely to the centroid of severe weather reports for the event (Fig. 6, inset map).

A weaker single-day signal (lower grid count) from CFSv2 guidance is shown for the six daily forecasts leading up to 13 April 2014 (Fig. 8). This event featured a mix of primarily severe hail and wind reports, and six tornadoes rated no stronger than EF1. Forecast maps reveal some possibility of a bimodal event with the bulk of SCP ≥ 1 grids counted across Texas, Arkansas, and Louisiana; and a secondary corridor of SCP ≥ 1 evident over portions of the Midwest and Northeast (Fig. 9). The inconsistent nature of the location of SCP ≥ 1 from one forecast to the next is consistent with greater uncertainty where severe weather may occur. Subjectively, this event is verified well by the centroid of convective QPF in the CFSv2 forecasts. And, while the environment for supercells may have existed and was accurately forecast by the CFSv2 along the corridor from east of the Mississippi River to New England, a significant convective precipitation signal was not present across this corridor. The lack of spatial overlap between convective precipitation and SCP ≥ 1 in the forecasts could be viewed by the forecaster as detrimental to confidence for more widespread severe weather, as was the case for this event.

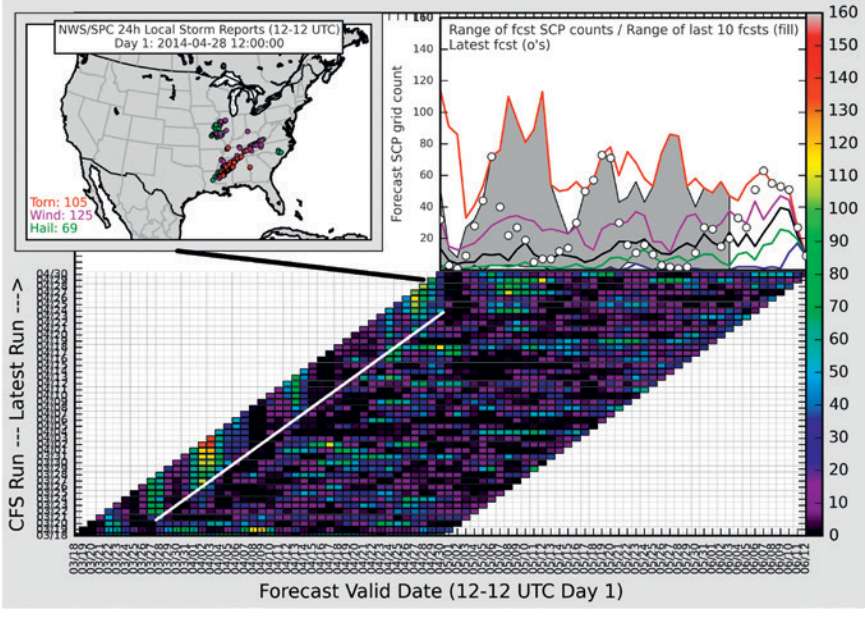

Fig. 10. As in Fig. 4, but for 28 Apr 2014.

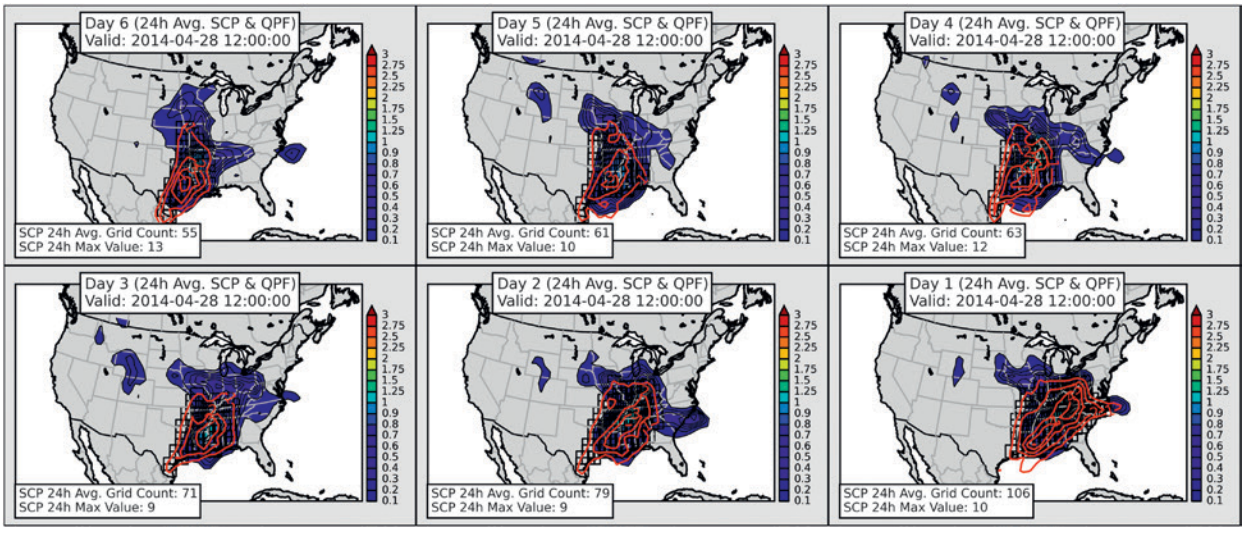

Fig. 11. As in Fig. 5, but for 28 Apr 2014.

The most active and significant severe weather day of the month occurred on 28 April 2014. This was the second of a multiday severe weather event, but the focus will be on the forecasts leading up to this particular day. More than 50 tornadoes were reported across six states, including eight tornadoes rated EF3, and one rated EF4. SCP ≥ 1 grid counts for this event begin to increase around 18 April 2014 (day-11 forecast). However, similar to the other events reviewed, a more consistent signal in SCP grid count magnitude commences between day 10 and day 7 (Fig. 10). Also, similar to the 3 April 2014 event, forecast grid counts exhibit a steady increase, from 55 on day 6 to over 100 on day 1 (Fig. 11). There is a distinct eastward shift in the area covered by SCP ≥ 1 and the strong convective QPF signal around day 3 is indicative of a faster system motion/evolution. However, the overall collocation of high values of SCP and convective QPF in forecasts from day 3 to day 1 correspond well with where significant severe weather occurred. Using the maps in conjunction with the trends in SCP ≥ 1 grid count/areal coverage can provide the forecaster with enhanced confidence in the magnitude of the severe weather event. While less significant, a smaller area where several severe wind and hail reports occurred across Missouri and Illinois was relatively well indicated by SCP ≥1 in the CFSv2 maps starting with the day 5 forecast for this event.

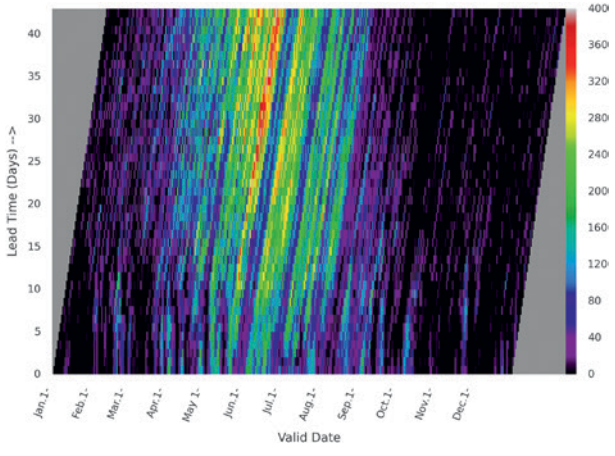

Fig. 12. All 2014 CFSv2 forecasts of SCP ≥ 1 grid counts from day 44 to day 1 (from the 0000 UTC CFSv2 ensemble mean).

UTILITY FOR WEEK 2 AND BEYOND.

Generally beyond a lead time of 7 days, the CFSv2 exhibits more run-to-run variability, providing a less consistent signal for an event (i.e., no vertical stripe on the chart). However, if SCP ≥ 1 grid counts are accumulated from run to run, then better signals emerge for some events beyond the first week. These events demonstrate the benefit of using past CFSv2 runs in a time-lagged ensemble approach. To illustrate this utility, the lead time is switched to the *y* axis, with each run of the CFSv2 along parallel diagonals (Fig. 12). Although there are few vertical stripes beyond day 10, there is a clear indication of the seasonality of severe weather. Taking a running (with respect to decreasing lead time) sum of all forecast SCP ≥ 1 grid counts verifying on the same day (Fig. 13) shows the strong seasonality of the CFSv2 ensemble mean of accumulated SCP ≥ 1, with the largest accumulated values peaking during June over the CONUS. Embedded in the plot are vertical spikes where runs of the CFSv2 have exhibited particularly favorable conditions

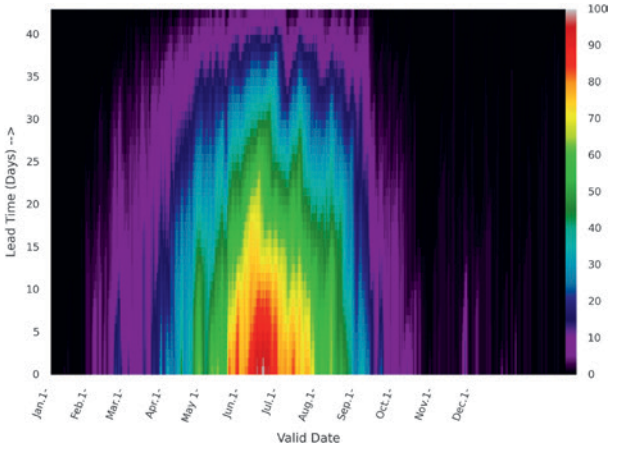

Fig. 13. Normalized running sum (over lead) of all forecast SCP ≥ 1 grid counts verifying on the same day produces a curve of CONUS-wide SCP.

(compared to a 2-week window) for severe weather over multiple runs (Fig. 14). Removing the mean of a 2-week window around each forecast day produces a forecast anomaly plot that reveals vertical stripes where forecast SCP counts have accumulated from multiple model runs (Fig. 15), indicating a relatively favorable severe weather environment. Note that diagonal features correspond to single forecast runs, and while they are present at long lead times, the accumulation method tends to smooth out run-to-run variability. The correlation of all positive anomaly forecasts to day-1 forecasts of positive anomaly (used as verification) appears to extend the consistency in these forecasts to at least 15 days (Fig. 3, green line). This approach nearly doubles the period of useful forecasts (correlation values above 0.5) compared to the single-day SCP grid count forecasts used in the Chiclet Chart.

Figure 16 provides subjective verification of positive anomaly forecasts for the period 8 January–14 May 2014. This portion of the year is used to assist in visualization. The underlying chart of positive anomalies is the same as shown in Fig. 15, only zoomed to 1 January–14 May 2014. The data for the first week of January 2014 are used in computing the mean of a 2-week window around each forecast day so that SCP positive anomaly forecasts commence on 8 January 2014. Semitransparent gray bars plotted over the colored positive anomaly forecasts indicate days with a significant number of observed hail and/or tornado events. Bars extending to half the *y* axis in Fig. 16 are days with a total number of severe hail and tornado events exceeding the daily mean (18) for the period 1 January–14 May 2014 but not exceeding one standard deviation above the mean. Bars fully encompassing the *y* axis are days with a total number of severe hail and tornado events exceeding one standard deviation above the mean (76 reports).

Weak false alarms appear in the positive anomaly forecasts on 11 and 14 January, when no significant severe weather was reported. More substantial false alarms appear from 3 to 5 February when normalized values in the range of 20–30 begin to appear in 5–7-day forecasts but no severe weather meeting our criteria is indicated. The stronger positive anomalies occurring on 21 and 22 February coincide with a couple of days of above-average severe weather (semitransparent gray bars extending to half the *y* axis in Fig. 16). The CFSv2 forecast signal for these 2 days begins to strengthen around 20–22 days in advance, fades, and then returns in the 5–10-day forecast range. These events are also followed by 3 days (22–24 February) with relatively strong positive anomaly forecasts but no severe weather indicated.

The multiday severe weather events observed around the beginning of April and reviewed above using the Chiclet Chart also show up well using the positive anomaly forecast approach. The 2–4 April events are characterized by less lead time than the 28 and 29 March events (27 March, while being an above-average severe weather day, was a missed forecast). The greatest positive anomalies of the entire year coincide with the significant severe weather events occurring at the end of April 2014. These events are preceded by a couple of above-average severe weather days that are poorly forecast (gray bars with no underlying color on 21 and 23 April). With the exception of 26 April, positive anomaly forecasts for the period 24–30 April all verified with above or much-above-normal severe weather activity. The greatest normalized positive anomaly of 100 occurs on 28 April, a day with the highest total number of significant tornadoes in

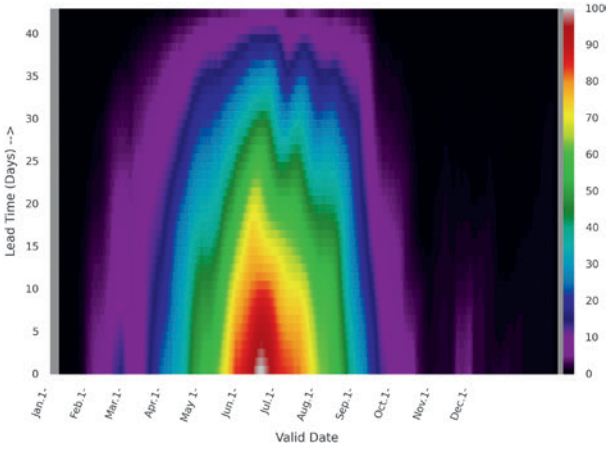

Fig. 14. Normalized 2-week-average window centered on each daily forecast of summed SCP grid counts.

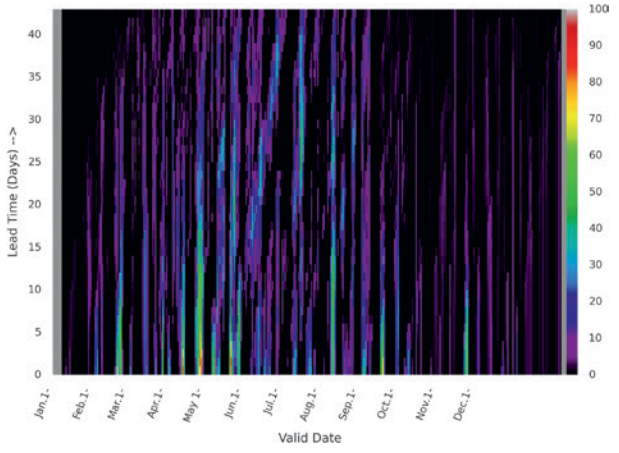

Fig. 15. Normalized cumulative grid count positive anomaly forecast. The result of subtracting the data in Fig. 14 from that in Fig. 13.

2014 (21 tornadoes rated EF2 or stronger). Positive anomaly forecasts for these active severe weather days at the end of April begin to appear around day 40 but values are not substantially discernable from other active and false-alarm days until around day 21, 3 weeks prior to the events, when positive anomaly values around 30 are indicated. Large anomalies can begin at these long forecast lead times but can also fade as the verification date approaches. However, in the case of late April, the amplitude of the positive anomaly increases, indicating continuing support from subsequent forecasts leading up to the event.

The positive anomaly forecast method also appears to exhibit skill in depicting the lack of supportive environments for severe weather. This is shown best during the period 1–6 May, when the lack of any severe weather events of significance corresponds well with near-zero-value anomaly forecasts. The positive anomaly signal returns and persists from 7 to 13 May and coincides well with a string of significant severe weather days (gray bars extending along the entire *y* axis in Fig. 16). A number of these forecasts exhibit relatively short lead times of 5–7 days, or generally weak long-lead positive anomaly forecasts. The final day of the time series shown in Fig. 16 is 14 May, a day with a significant number of severe weather events but a fading signal in the positive anomaly forecast.

These examples demonstrate that while consecutive daily forecasts may exhibit large inconsistency at long lead times (Fig. 12), there may still be utility from the CFSv2 forecasts regarding favorable severe weather environments beyond 1 week by accumulating grid counts of SCP ≥ 1 and by applying a time-averaging technique to derive forecast anomalies as described here.

CONCLUSIONS AND CONTINUING RESEARCH. The Chiclet Chart and accompanying maps of SCP areal coverage demonstrate the predictive skill of the CFSv2 for identifying severe weather events based on environments with large CAPE and strong vertical wind shear, as indicated by SCP values ≥ 1. For days reviewed during March–April 2014, the CFSv2 showed consistent forecasts of SCP coverage beginning around 7 days before the severe weather events.

Once the CFSv2 indicates a possible upcoming event, further investigation is needed in order to ensure skillful severe weather prediction. Ensemble averaging across several runs may help increase confidence and lead time. In addition, synoptic- and larger-scale pattern recognition within a CFSv2 ensemble mean is important for evaluating severe weather potential. Other environmental factors should also be considered, as well as parameter normalizations calibrated specifically to CFSv2 climatology. For example, high-SCP environments can accompany both capped days with no convection and uncapped days with widespread interfering convective cells. Considering convective inhibition (CIN) and convective QPF along with SCP should also provide the forecaster with additional information and confidence in making extended-range forecasts for severe convection.

Beyond 7 days, run-to-run consistency decreases substantially. The patterns observed on the Chiclet Chart in this situation are composed of more horizontal streaks than vertical streaks. The horizontal streaks are

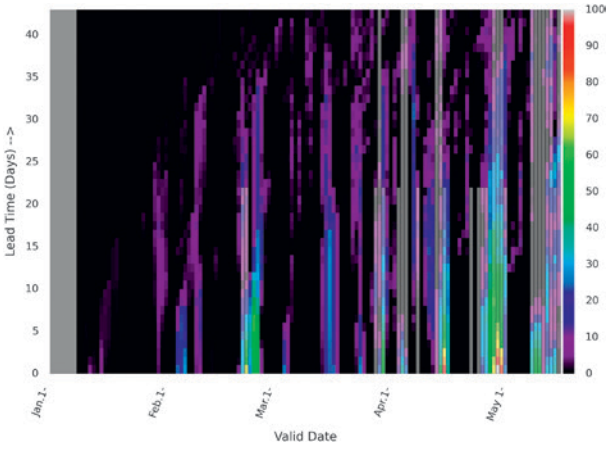

Fig. 16. Underlying colored chart as in Fig. 15, but zoomed to period from 1 Jan to 14 May 2015. Overlying semitransparent gray vertical bars are days with above average (half bar) or more than one standard deviation above average (full bar) severe hail and tornado reports. Data for the first week of Jan 2014 are used in computing the mean of a 2-week window so that SCP positive anomaly forecasts commence on 8 Jan 2014.

indicative of periods of favorable environmental conditions for severe weather on a synoptic time scale. These regimes tend to be characterized by positive feedback, such that the synoptic pattern favorable for strong convection is repeated. As a result, consecutive model runs can exhibit drastic differences from week 2 and beyond.

Despite the run-to-run variability, signals in the extended range can be extracted by integrating the SCP ≥ 1 grid counts across all forecast runs. This approach reveals long vertical spikes on the chart, where past runs of the CFSv2 produced greater coverage of SCP ≥ 1 for the same day. This visualization method serves as a supplement to the Chiclet Chart by highlighting days at extended lead times that require attention in future forecast runs. Following the implementation of these real-time products, the use of the visualization methods presented here will be expanded to include different forecast models and forecast variables.

ACKNOWLEDGMENTS. This study was supported by NOAA Award NA14OAR4310185, the Office of Naval Research Award N00014-12-1-091, and a Columbia University Research Initiatives for Science and Engineering (RISE) award. S. Lillo's contribution was supported under NOAA-OAR-CPO Grant 2014-2003692. The views expressed herein are those of the authors and do not necessarily reflect the views of NOAA or any of its subagencies. We wish to thank Israel Jirak of SPC for his thorough review of the manuscript prior to submission and three reviewers for their constructive comments and suggestions to improve this work.

REFERENCES

Allen, J. T., M. K. Tippett, and A. H. Sobel, 2015: Influence of the El Niño/Southern Oscillation on tornado and hail frequency in the United States. *Nat. Geosci.*, **8**, 278–283, doi:10.1038/ngeo2385.

Barnston, A. G., M. K. Tippett, M. L. L'Heureux, S. Li, and D. G. DeWitt, 2012: Skill of real-time seasonal ENSO model predictions during 2002–11. Is our capability increasing? *Bull. Amer. Meteor. Soc.*, **93**, 631–651, doi:10.1175/BAMS-D-11-00111.1.

Brooks, H. E., J. W. Lee, and J. P. Craven, 2003: The spatial distribution of severe thunderstorm and tornado environments from global reanalysis data. *Atmos. Res.*, **67–68**, 73–94, doi:10.1016/S0169-8095(03)00045-0.

Camargo, S. J., A. G. Barnston, P. J. Kotzbach, and C. W. Landsea, 2007: Seasonal tropical cyclone forecasts. *WMO Bull.*, **56**, 297–309.

Doswell, C. A., III, 1980: Synoptic-scale environments associated with High Plains severe thunderstorms. *Bull. Amer. Meteor. Soc.*, **61**, 1388–1400, doi:10.1175/1520-0477(1980)061<1388:SSEAWH>2.0.CO;2.

——, and D. M. Schultz, 2006: On the use of indices and parameters in forecasting severe storms. *Electron. J. Severe Storms Meteor.*, **1** (3). [Available online at www.ejssm.org/ojs/index.php/ejssm/article/viewarticle/11/12.]

Grams, J. S., R. L. Thompson, D. V. Snively, J. A. Prentice, G. M. Hodges, and L. J. Reames, 2012: A climatology and comparison of parameters for significant tornado events in the United States. *Wea. Forecasting*, **27**, 106–123, doi:10.1175/WAF-D-11-00008.1.

Kirtman, B. P., and M. Dughong, 2009: Multimodel ensemble ENSO prediction with CCSM and CFS. *Mon. Wea. Rev.*, **137**, 2908–2930, doi:10.1175/2009MWR2672.1.

Saha, S., and Coauthors, 2014: The NCEP Climate Forecast System version 2. *J. Climate*, **27**, 2185–2208, doi:10.1175/JCLI-D-12-00823.1.

Thompson, R. L., R. Edwards, J. A. Hart, K. L. Elmore, and P. Markowski, 2003: Close proximity soundings within supercell environments obtained from the Rapid Update Cycle. *Wea. Forecasting*, **18**, 1243–1261, doi:10.1175/1520-0434(2003)018<1243:CPSWSE>2.0.CO;2.

——, C. M. Mead, and R. Edwards, 2007: Effective storm-relative helicity and bulk shear in supercell thunderstorm environments. *Wea. Forecasting*, **22**, 102–115, doi:10.1175/WAF969.1.

Tippett, M. K., A. G. Barnston, and S. Li, 2012a: Performance of recent multimodel ENSO forecasts. *J. Appl. Meteor. Climatol.*, **51**, 637–654, doi:10.1175/JAMC-D-11-093.1.

——, A. H. Sobel, and S. J. Camargo, 2012b: Association of U.S. tornado occurrence with monthly environmental parameters. *Geophys. Res. Lett.*, **39**, L02801, doi:10.1029/2011GL050368.

——, J. T. Allen, V. A. Gensini, and H. E. Brooks, 2015a: Climate and hazardous convective weather. *Curr. Climate Change Rep.*, **1**, 60–73, doi:10.1007/s40641-015-0006-6.

——, M. Almazroui, and I.-S. Kang, 2015b: Extended-range forecasts of areal-averaged Saudi Arabia rainfall. *Wea. Forecasting*, **30**, 1090–1105, doi:10.1175/WAF-D-15-0011.1.

Radar and Atmospheric Science: A Collection of Essays in Honor of David Atlas

Edited by Roger M. Wakimoto and Ramesh Srivastava

This monograph pays tribute to one of the leading scientists in meteorology, Dr. David Atlas. In addition to profiling the life and work of the acknowledged "Father of Radar Meteorology," this collection highlights many of the unique contributions he made to the understanding of the forcing and organization of convective systems, observation and modeling of atmospheric turbulence and waves, and cloud microphysical properties, among many other topics. It is hoped that this text will inspire the next generation of radar meteorologists, provide an excellent resource for scientists and educators, and serve as a historical record of the gathering of scholarly contributions honoring one of the most important meteorologists of our time.

Radar and Atmospheric Science: A Collection of Essays in Honor of David Atlas

Aug 2003. Meteorological Monograph Series, Vol. 30, No. 52; 270 pp, hardbound; ISBN 1-878220-57-8; AMS code MM52.

Price $80.00 member

To place an order point your Web browser to www.ametsoc.org/amsbookstore

AMS BOOKS

RESEARCH ◆ APPLICATIONS ◆ HISTORY